Influence of Debye plasmas on photoionization of Li-like ions: Emergence of Cooper minima

C. Y. Lin* and Y. K. Ho

Institute of Atomic and Molecular Sciences, Academia Sinica, Taipei 106, Taiwan

(Received 25 November 2009; published 8 March 2010)

The photoionizaton processes of lithium isoelectronic sequence (Be^+, B^{2+}, C^{3+}, N^{4+}, O^{5+}, and F^{6+}) under the influence of plasma environments are explored using the method of complex coordinate rotation in combination with the model potential approximation. The photoionization cross sections compared to existing theoretical predictions and varied with Debye screening lengths are reported. Under the perturbation of plasmas with certain Debye screening lengths, Cooper minima are uncovered in photoionization cross-section curves of the ground-state Li-like ions, in which the Cooper minima are absent in the respective free ion cases. The relations between the appearance of Cooper minima and the instability of the ground states due to plasma environments are discussed.

DOI: 10.1103/PhysRevA.81.033405 PACS number(s): 32.80.Fb, 52.20.Hv

I. INTRODUCTION

Photoionization of atoms or ions as a probe of electronic correlation is of importance to understand complex physical systems. The interpretation of spectroscopic observation or theoretical modeling for astrophysical objects [1–3] particularly relies on accurate atomic data, such as photoionization cross sections, transition probabilities, and energy levels. The focus of the present investigation is photoionization processes of the lithium isoelectronic sequence under the influence of Debye plasmas. Although many theoretical calculations [4–7] and experimental data [8] of lithium photoionization have been reported, the influence of plasma screening effects on photoionization of Li-like ions were relatively unexplored. To shed further light on such an issue, we investigate the lithium isoelectronic sequence using the method of complex coordinate rotation in combination with the model potential approximation to clarify the effects due to plasma environments.

Understanding atomic processes in plasmas has been known as an important issue for many different physical systems from nanoscale devices to astrophysical objects, since it could provide useful diagnostics in a variety of plasma properties. The plasma environments are anticipated to affect the atomic processes significantly due to screening effects. In recent years, there has been considerable effort devoted to investigations of atomic photoionization processes in plasma environments [9–13], because photoionization is extremely sensitive to the details of atomic structure and electronic correlation effects.

The recent studies on photoionization processes in Debye plasmas by Sahoo and Ho [10,12] firstly discovered that Cooper minima appear in photoionization cross sections of ground-state lithium due to plasma screening effects. It has been well known that there is no Cooper minimum existing in cross-section curves of ground-state lithium, even though the $2s$ state wave function of lithium has one node. The existence of Cooper minimum in plasma-embedded lithium also has been demonstrated by the theoretical work of Qi *et al.* [13].

The Cooper minima occurring in photoionization cross sections of neutral atoms without screening of plasmas are realized by the departure of discrete and continuum wave functions from hydrogen-like behavior, because the hydrogen atom shows no minima in any state. The plasma screening effects, which could result in more deviation of wave functions than unscreened atoms or ions, are expected to provide a further adjustment of distribution of wave functions causing the complete cancellation of dipole matrix elements.

Calculations have been performed for the lithium isoelectronic sequence of Be^+, B^{2+}, C^{3+}, N^{4+}, O^{5+}, and F^{6+}. The discussions of the theoretical method and its applications to the photoionization processes in plasmas are described in Sec. II. The results of photoionization for each ion are presented and discussed in Sec. III and a summary and conclusions are given in Sec. IV. Atomic units are used throughout, unless otherwise noted.

II. THEORETICAL METHOD

A. The method of complex coordinate rotation

In the early 1970s, a number of studies, such as the work by Broad and Reinhardt [14], proposed that photoionization profiles might be obtained through the frequency-dependent polarizability utilizing conventional bound-state techniques. In 1975, a rigorous approach based on the method of complex coordinate rotation was developed by Rescigno and McKoy [15] for calculations of photoionization cross sections. The theoretical perspectives and applications of this method to atomic and molecular systems had been reviewed and discussed in articles by Reinhardt [16,17] and Ho [18], respectively. In addition, the discussion of crucial features of resonance wave functions and electronic density can be found in the review article by Buchleitner *et al.* [19]. In the present article, only brief description of the method is given.

In the electric dipole approximation, the photoionization cross sections are given by

$$\sigma(\omega) = \frac{4\pi\omega}{c}\mathrm{Im}[\alpha^-(\omega)], \quad (1)$$

*cylin@pub.iams.sinica.edu.tw

where $\alpha^-(\omega)$ is the negative frequency component of the polarizability [15], ω the photon energy, and c the speed of light (i.e., the inverse fine-structure constant). To evaluate $\alpha^-(\omega)$ solely in the bound-state-type basis set, we perform the transformation of radial coordinates,

$$r \to r\Theta, \tag{2}$$

where

$$\Theta = \exp(i\theta). \tag{3}$$

Within the framework of the complex coordinate rotation, the negative frequency component of the polarizability $\alpha^-(\omega)$ for atomic systems in a stationary state ψ_0 with energy E_0 becomes [20],

$$\alpha^-(\omega) = \sum_i \Theta^3 \frac{\int d^3r\, \psi_0^\dagger(r\Theta)\mu(r\Theta)\psi_i(r) \int d^3r\, \psi_i^\dagger(r)\mu(r\Theta)\psi_0(r\Theta)}{E_i - E_0 - \omega}, \tag{4}$$

where μ is the component of dipole operator in the direction of the polarization of light. In the present calculations, the wave function $\psi_0(r\Theta)$ is obtained by an unrotated Hamiltonian and then transformed into complex coordinates of the radial variable, while the wave functions $\psi_i(r)$ consisting of linear combinations of real discrete basis functions (unrotated basis functions) with complex coefficients are acquired from a rotated Hamiltonian. The eigenvalues E_i corresponding to ψ_i are complex. Note that the conjugate functions $\psi_0^\dagger$ and $\psi_i^\dagger$ are defined by taking the complex conjugate of angular part only, but not of radial part.

To obtain required wave functions and energies in Eq. (4), we need to solve the complex scaled nonrelativistic Hamiltonian equation with

$$H(r\Theta) = -\Theta^{*2}\frac{1}{2}\nabla^2 + \Theta^* V(r), \tag{5}$$

in which the ordinary potential and kinetic operators are scaled by Θ^*, the complex conjugate of Θ, and Θ^{*2}, respectively. The trial wave functions are expanded in terms of N linear independent basis functions,

$$\psi_i = \sum_{k=0}^{N-1} c_k^i \chi_k. \tag{6}$$

In the present calculations, the Slater-type basis functions,

$$\chi_k(r, \vartheta, \varphi; \xi) = r^{l+k}\exp(-\xi r)Y_{l,m}(\vartheta, \varphi), \tag{7}$$

with ξ being a variational parameter and $Y_{l,m}$ being the spherical harmonics are adopted for the computing advantage of Hamiltonian matrix elements. The basis functions with different quantum number l are orthogonal due to the orthogonality of the spherical harmonics. Taking advantage of the trial wave functions, the complex eigenvalue equations can be obtained using the generalized variational approach. The eigen equations expressed in the matrix representation are

$$\mathbf{H}(r\Theta)\mathbf{C}_i = E_i\mathbf{N}\mathbf{C}_i, \tag{8}$$

where $\mathbf{H}(r\Theta)$ and $\mathbf{N}$ are the complex scaled Hamiltonian and overlap matrices, while E_i are complex eigenvalues and $\mathbf{C}_i$ are complex eigenvectors with components of $\{c_0^i, c_1^i, \ldots, c_{N-1}^i\}$. It is worth noticing that the overlap matrix elements $\mathbf{N}_{ij}$, defined as

$$\mathbf{N}_{ij} = \langle\chi_i|\chi_j\rangle, \tag{9}$$

are nonzero for $i \neq j$ because of the nonorthogonal property of Slater-type basis functions. To solve the so-called generalized eigenvalue problem, the decomposition of $\mathbf{N}$ is necessary for numerical stability.

The method of complex coordinate rotation had been widely and successfully employed to study the atomic processes in strong electric field [21] and plasma environments [9–12]. It is well known that resonance phenomena frequently occur in various atomic and molecular processes, such as electron-atom scattering and atomic photoionization. This method, in which resonance parameters, such as resonance positions and widths, can be obtained using L^2 (square-integrable) basis sets exclusively appears to have a great computational advantage.

B. The model potential

To reduce the computational cost, the model potential method is utilized providing not only a simpler way to study multielectron systems, but also physical interpretations to understand complex phenomena. For the cases of one electron in the field of a $1s^2$ core, the model potential proposed by Bachau *et al.* [22] has been extensively and successfully adopted to explore the three-electron systems. In this model, the multielectron atom or ion is treated as a combination of one valence electron and an atomic ion core. The interaction between the valence electron and the core is described by a model potential $V_m(r)$, which can generate a good approximation for the direct and exchange potentials of the Hartree-Fock equations. The electrostatic potential of a core with nuclear charge Z and composed of two $1s$ electrons is defined in atomic units by

$$V(r) = -\frac{Z}{r} + V_m(r), \tag{10}$$

where the model potential $V_m(r)$ is expressed in the form of

$$V_m(r) = \frac{2}{r} - \frac{2}{r}(1 + \alpha r)\exp(-2\alpha r). \tag{11}$$

The potential $V(r)$ verifies the correct asymptotic conditions,

$$V(r) \sim \begin{cases} -\frac{Z-2}{r} & \text{for} \quad r \to \infty; \\ -\frac{Z}{r} & \text{for} \quad r \to 0. \end{cases} \tag{12}$$

The parameter α in inverse Bohr radii is determined by fitting the second lowest eigenvalues of the Hamiltonian equation to

TABLE I. The model potential parameters α fitted to reproduce the experimental first ionization energies.

	Fitted parameter α	First ionization energies Expt. data[a] (cm^{-1})
Be^{+}	2.35184193	146882.86
B^{2+}	3.04214788	305931.10
C^{3+}	3.72763815	520178.4
N^{4+}	4.40613024	789532.9
O^{5+}	5.07406907	1114008
F^{6+}	5.72917743	1493629

[a]Ref. [23].

the experimental energy of the $1s^2 2s\ ^2S$ ground state. Table I gives the parameters α used in this work for Li-like ions, which exactly reproduce the experimental data [23] for the ground-state energies of ions with respect to their next-higher-stage ions (i.e., the first ionization energies).

For the investigation of Li-like ions in plasma environments, the interaction potentials involving the plasma screening effects based on the Debye-Hückel model are given by [24]

$$V_{sc}(r) = V(r)\exp(-r/\lambda_D), \tag{13}$$

where $V(r)$ is defined in Eq. (10) and λ_D is the Debye screening length in Bohr radii (a_0). To understand the plasma screening effects on photoionization processes of Li-like ions, the screened potential $V_{sc}(r)$ is utilized instead of $V(r)$ in Eq. (5). In the present model, we consider the exchange effects of the photoelectron with the core electrons, but without the plasma electrons. In weakly coupled Debye plasmas where the plasma electron densities are low, the lowering of ionization potential [25,26] due to this effect is expected to be relatively small and not to affect the overall profile of photoionization cross sections. For strongly coupled plasmas, in which the number density of plasma electrons is high, and the ion-sphere model is used instead of the Debye-Hückel model to represent the atomic interaction potential, the exchange effect between the atomic electron and the plasma electrons may have larger effect on the lowering of continuum.

III. RESULTS AND DISCUSSION

With the aid of model potentials, we investigate photoionization processes of lithium isoelectronic sequence from $Z = 4$ to 9 using the method of the complex coordinate rotation. To study the influence of plasma environments on ground-state photoionization, the screening effects due to plasmas are described by the Debye-Hückel model. The calculations are performed in the Slater-type basis functions and the parameters ξ used in Eq. (7) are determined by the variational principle for energy spectra to obtain the optimized basis functions. In evaluating energy spectra and photoionization cross sections, the number of basis functions between 30 and 35 is sufficient for the present cases to reach convergent results. In the present results, the photoionization cross sections are calculated in the dipole-length approximation.

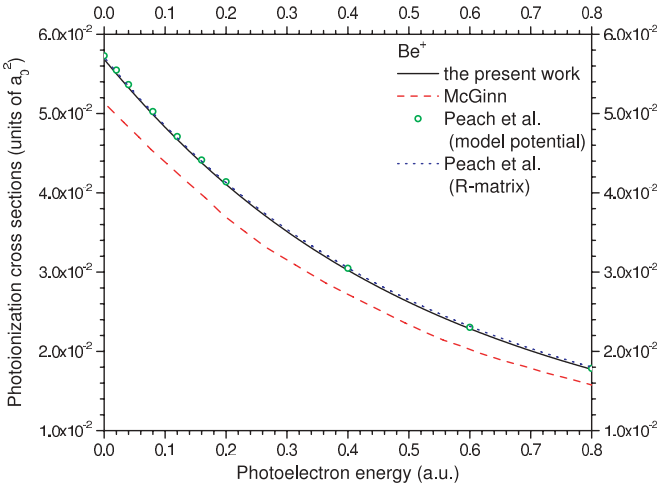

FIG. 1. (Color online) Photoionization cross sections of the ground state of Be^{+} ions calculated in the present work are compared to the theoretical results by McGinn [4] and Peach *et al.* [7].

A. Be^{+}

To verify the validity of the present approach, our results of photoionization cross sections from the ground state for free Be^{+} ions that correspond to $\lambda_D \to \infty$ are compared to available theoretical data by McGinn [4] and Peach *et al.* [7] in Fig. 1. The photoionization cross sections predicted by McGinn [4] adopt the pseudopotential method in the dipole-velocity approximation. The results of Peach *et al.* [7] are obtained using two theoretical methods, the model potential and close-coupling *R*-matrix, respectively. The model potential is represented in the analytic form,

$$V(r) = -\frac{Z-2}{r} - \frac{2}{r}(1+\delta x+\delta' x^2)\exp(-\gamma x) - \frac{\alpha_d}{2r^4}\omega_2(\beta x); \quad x = (Z-2)r, \tag{14}$$

where α_d is the static dipole polarizability of the core, ω_2 the cutoff function, and γ, δ, δ', and β are empirical coefficients. The detailed information of parameters and functions for this model potential can be found in Ref. [7]. Our results compared to those in model potential and close-coupling *R*-matrix calculations by Peach *et al.* [7] are in very good agreement, but are much larger than data by McGinn [4]. It is worth mentioning that except for McGinn [4] using the dipole-velocity formulation, all calculations adopt the dipole-length formulation.

In Fig. 2, the photoionization cross sections of plasma-embedded Be^{+} ions as functions of Debye screening lengths are displayed for illustration of the plasma screening effects. It obviously shows that photoionization cross sections, near the threshold region in particular, are quite sensitive to plasma environments. It is seen that no Cooper minimum occurs for the case of isolated Be^{+} ions ($\lambda_D \to \infty$) as expected. With decreasing of the Debye screening length, however, the threshold cross sections are depressed gradually. A Cooper minimum begins to appear very close to the ionization threshold in photoionization cross sections when λ_D is decreased to about 3.0. The further decrease of λ_D causes the location of Cooper minimum to move toward the higher energies, while cross

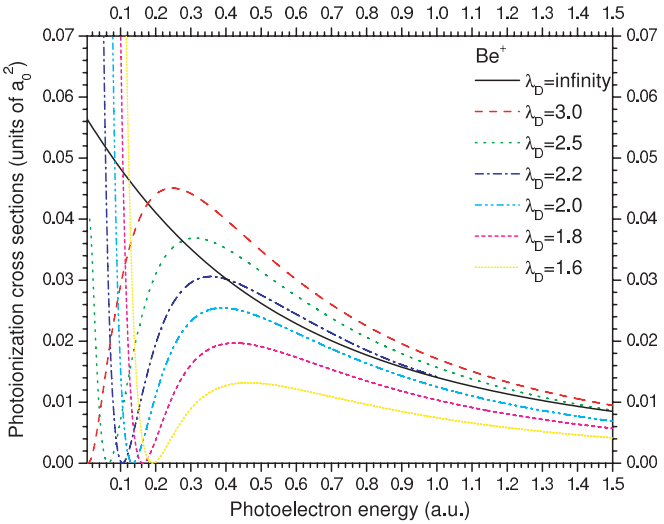

FIG. 2. (Color online) Photoionization cross sections of the ground state of Be^+ ions varied with different Debye screening lengths λ_D (units of a_0).

sections near the threshold grow sharply and the humps to the right of Cooper minima are reduced.

It is well known that the appearance of Cooper minima is mainly due to the cancellation of positive and negative contributions from discrete and continuum wave functions in the dipole matrix elements. Since the $2s$ wave function has one node and the ϵp wave function becomes more compact with the increase of photon energy ϵ, it seems that in the transition of $2s \rightarrow \epsilon p$, the negative and positive components of the dipole transition matrix element just cancel each other at some photon energy. Although it does not occur in ground-state photoionization of free Be^+ ions, the deviation of atomic wave functions from the behavior of free Be^+ ions induced

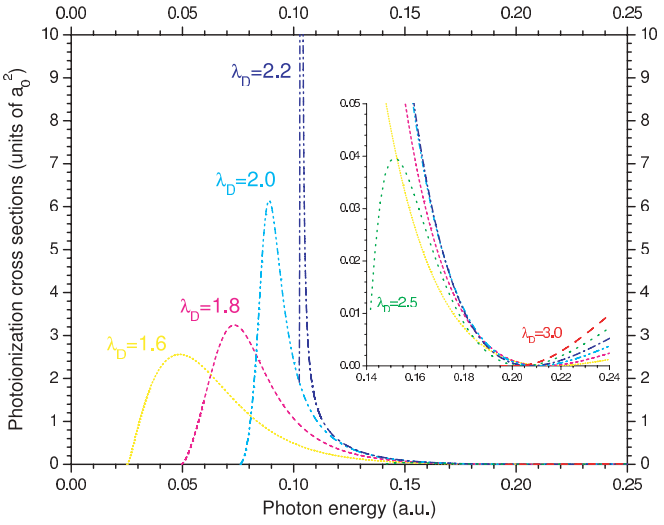

FIG. 3. (Color online) Photoionization cross sections near ionization thresholds of the ground state of Be^+ ions as functions of photon energies for several Debye screening lengths λ_D (units of a_0). Each curve starts from the photon energy at its ionization threshold. The inset shows the detailed behavior of cross sections for photon energies from 0.14 to 0.24 a.u.

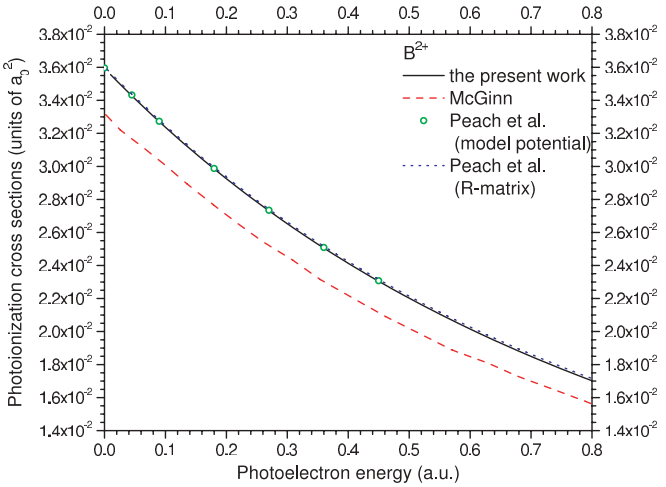

FIG. 4. (Color online) Photoionization cross sections of the ground state of B^{2+} ions calculated in the present work are compared to the theoretical results by McGinn [4] and Peach *et al.* [7].

by the plasma screening effects increases the possibility for cancellation.

In Fig. 3, we emphasize the photoionization cross sections near the ionization thresholds as functions of photon energies instead of the photoelectron energies. The cross sections are zero at their respective ionization thresholds, with the exception of $\lambda_D = 2.2$ and 2.5. The inset of Fig. 3 shows the relatively small cross sections for $\lambda_D = 2.5$ and 3.0. It can be observed that shape resonances due to the quasibound $2p$ states occur for λ_D in between 1.6 and 2.2, because the $2p$ state shifts toward the ionization threshold with decreasing λ_D and becomes unbound as $\lambda_D \sim 2.2$.

We perform the calculations of oscillator strengths for the Be^+ ion case as an example to confirm the sum rules of oscillator strengths in the current approach. Since the existence of np bound states, in which n is the principal quantum number, depends on the Debye screening lengths, there is only one bound state that can exist for $\lambda_D = 2.5$ and 3.0, but not any

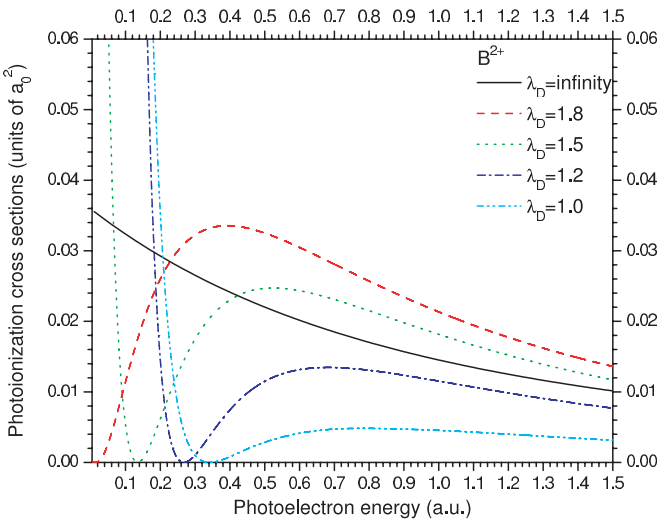

FIG. 5. (Color online) Photoionization cross sections of the ground state of B^{2+} ions varied with different Debye screening lengths λ_D (units of a_0).

TABLE II. The sum of oscillator strengths for screened Be^+ ions in different Debye screening lengths λ_D. ϵ is the energy of the ejected electron. Only one $2p$ bound state at most could exist for λ_D between 1.6 and 3.0.

λ_D (units of a_0)	$2s \rightarrow \epsilon p$	$2s \rightarrow 2p$	Sum
1.6	0.9968	0.0	0.9968
1.8	0.9961	0.0	0.9961
2.0	0.9993	0.0	0.9993
2.2	0.9980	0.0	0.9980
2.5	0.3010	0.6973	0.9983
3.0	0.3484	0.6495	0.9979

bound states for λ_D in between 1.6 and 2.2. According to the sum rules for the present case, which is equivalent to the one-electron case, the summation of oscillator strengths equal to one should be fulfilled. The results for different Debye screening lengths are given in Table II. The bound-bound and bound-free oscillator strengths are summed up within 0.4% deviation from 1.

B. B^{2+}

The present results of ground-state photoionization cross sections for free B^{2+} ions compared to other theoretical calculations [4,7] are presented in Fig. 4. Our work has good agreement with those by Peach *et al.* [7], but some discrepancy with the work by McGinn [4]. The photoionization cross sections of plasma-embedded B^{2+} ions as functions of Debye screening lengths are given in Fig. 5 for demonstration of the plasma screening effects. There is still no Cooper minimum existing in the case of free B^{2+} ions, but it begins to appear near the ionization threshold in photoionization cross sections as $\lambda_D = 1.8$. The variation of Cooper minimum locations is dependent on plasma screening. In the B^{2+} case, the Cooper minima only exist in the range of λ_D between around 1.0 and 1.8. For λ_D less than 1.0, the screening effect is so strong that the ground state is extremely close to the ionization threshold. On the contrary, as λ_D beyond 1.8, the screening effect is relatively weak such that the departure of atomic wave functions from isolated B^{2+} ions induced by plasma environments could not provide a complete cancellation of the dipole matrix element.

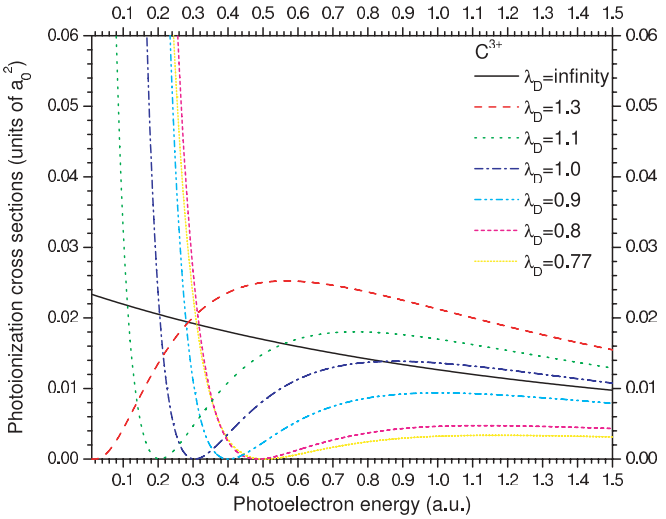

FIG. 7. (Color online) Photoionization cross sections of the ground state of C^{3+} ions varied with different Debye screening lengths λ_D (units of a_0).

C. C^{3+}

In Fig. 6, the comparison of the present work with available theoretical predictions is given. The ground-state photoionization cross sections of free C^{3+} ions in the present calculations are in excellent agreement with results by Peach *et al.* [7] and Nahar and Pradhan [27]. The nonrelativistic close-coupling approximation using the *R*-matrix method is performed by Peach *et al.* [7] and Nahar and Pradhan [27] successively. In the calculations of Nahar and Pradhan [27], however, the total wave function is given by an 11-state

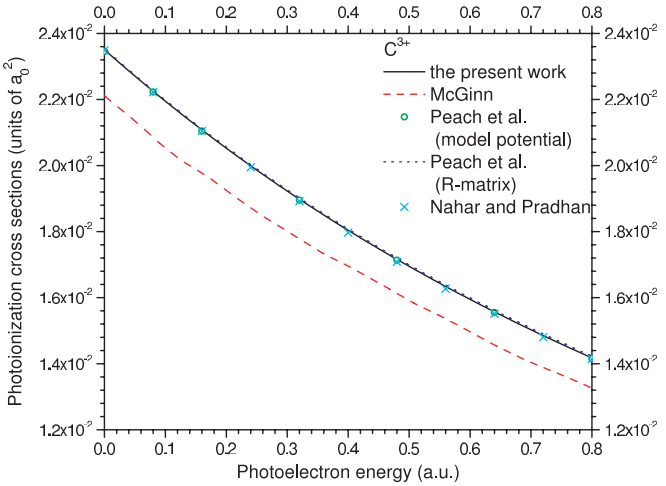

FIG. 6. (Color online) Photoionization cross sections of the ground state of C^{3+} ions calculated in the present work are compared to the theoretical results by McGinn [4], Peach *et al.* [7], and Nahar and Pradhan [27].

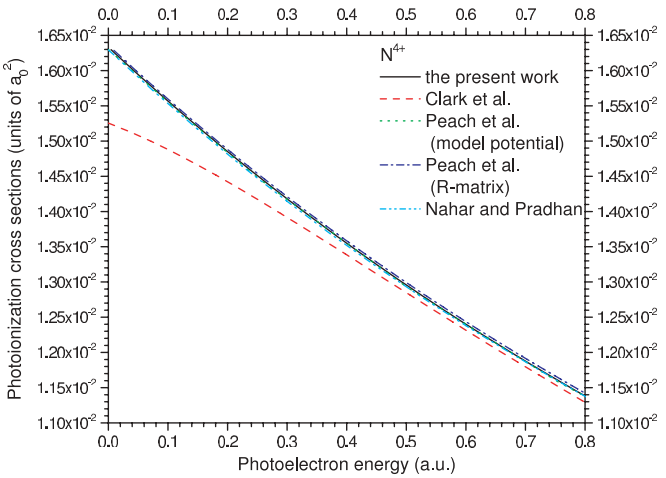

FIG. 8. (Color online) Photoionization cross sections of the ground state of N^{4+} ions calculated in the present work are compared to the theoretical results by Clark *et al.* [6], Peach *et al.* [7], and Nahar and Pradhan [27].

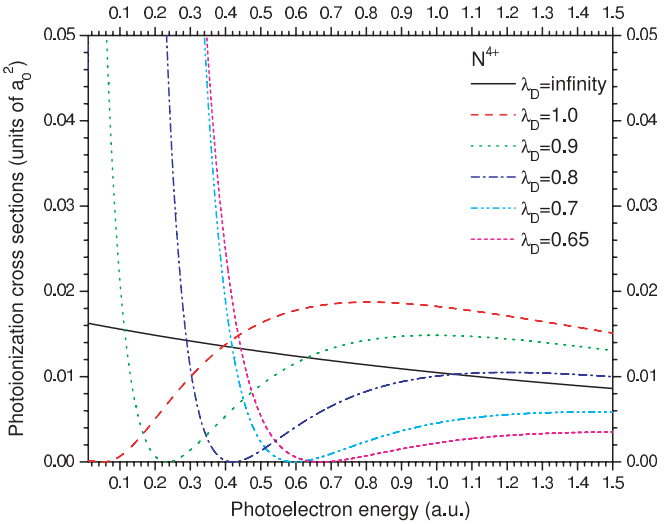

FIG. 9. (Color online) Photoionization cross sections of the ground state of N^{4+} ions varied with different Debye screening lengths λ_D (units of a_0).

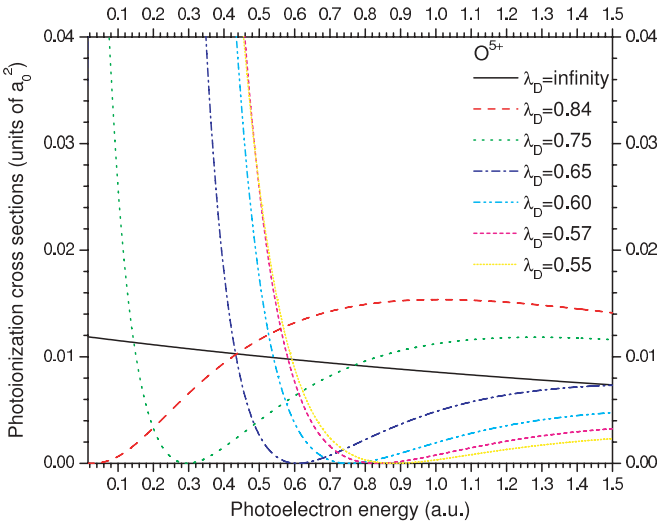

FIG. 11. (Color online) Photoionization cross sections of the ground state of O^{5+} ions varied with different Debye screening lengths λ_D (units of a_0).

expansion instead of a two-state expansion, which is employed in the work by Peach *et al.* [7]. The photoionization cross sections of plasma-embedded C^{3+} ions varied with Debye screening lengths given in Fig. 7 display the Cooper minima existing only in between $\lambda_D = 0.77$ and 1.3. It apparently shows that cross sections are dominated by transitions of photoelectron energies smaller than the Cooper minimum energy as plasma screening effects are enhanced. In the case of $\lambda_D = 0.77$, for instance, while the ground state shifts toward the ionization threshold due to the strong influence of plasma screening, the cross sections drop steeply for energies approaching the Cooper minimum from the low-energy region and retain in relative low values for energies larger than the Cooper minimum.

D. N^{4+}

Figure 8 compares the present work to the theoretical predictions by Clark *et al.* [6], Peach *et al.* [7], and Nahar and Pradhan [27]. In the calculations of Clark *et al.* [6], the configuration-averaged photoionization cross sections are obtained in the single configuration approximation using the Hartree-Fock relativistic method. The nonrelativistic close-coupling *R*-matrix method is carried out successively by Peach *et al.* [7] utilizing a two-state expansion and by Nahar and Pradhan [27] using an 11-state expansion of total wave functions. To study the influence of plasma environments on photoionization of N^{4+} ions, the photoionization cross sections are computed in the Debye-Hückel model with various Debye screening lengths. In Fig. 9, the photoionization cross sections are dramatically changed when the Cooper minima are uncovered for λ_D in between 0.65 and 1.0.

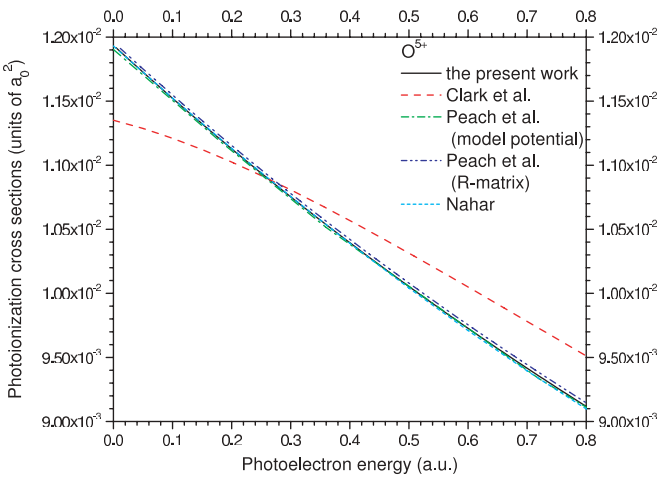

FIG. 10. (Color online) Photoionization cross sections of the ground state of O^{5+} ions calculated in the present work are compared to the theoretical results by Clark *et al.* [6], Peach *et al.* [7], and Nahar [28].

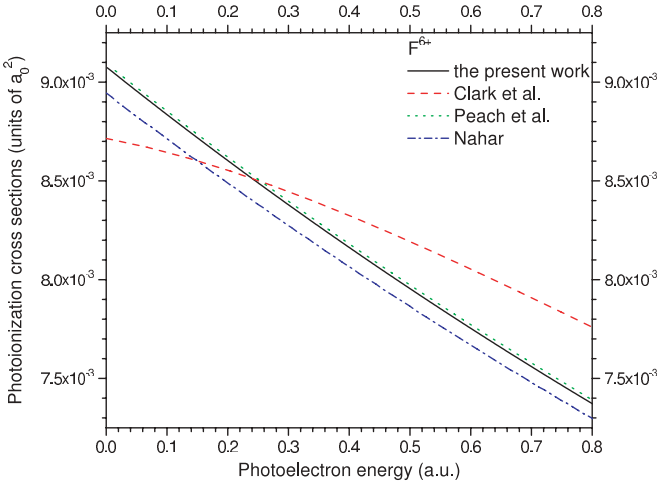

FIG. 12. (Color online) Photoionization cross sections of the ground state of F^{6+} ions calculated in the present work are compared to the theoretical results by Clark *et al.* [6], Peach *et al.* [7], and Nahar [29].

E. O^{5+}

The present calculations of O^{5+} photoionization cross sections without screening effects of plasmas are presented in Fig. 10 and compared to other theoretical results. Our results are in good agreement with those by Peach *et al.* [7] and Nahar [28], but in some discrepancy with work by Clark *et al.* [6]. Similarly, Peach *et al.* [7] adopted a two-state and Nahar [28] employed an 11-state eigenfunction expansion in the nonrelativistic close-coupling *R*-matrix calculations. The photoionization cross sections of plasma-embedded O^{5+} ions as functions of Debye screening lengths are presented in Fig. 11 for illustration of the plasma screening effects. The Cooper minima of O^{5+} behave substantially the same manner as other Li-like ions. No Cooper minimum exists in the free O^{5+} case, but they appear for λ_D in between 0.55 and 0.84.

F. F^{6+}

In Fig. 12, the comparison of the present work with available theoretical predictions is given. The photoionization cross sections of isolated F^{6+} ions in the present calculations are in agreement with results by Peach *et al.* [7], but show some differences with the predictions by Clark *et al.* [6] and Nahar [29]. The difference between the present work and Nahar's results [29] might be due to the relativistic effect. In Nahar's calculations [29], the relativistic fine structure is considered through the Breit-Pauli *R*-matrix method. The influence of plasma environments on photoionization of F^{6+} ions is clarified in Fig. 13, where the Cooper minima appear for λ_D in between 0.46 and 0.7.

To summarize the results of above ions, the photoionization cross sections of unscreened Li-like ions for selected photoelectron energies obtained in the present work are given and compared with the available data in Tables III and IV. For the screened cases of some selected Debye screening lengths, the numerical data of photoionization cross sections as functions of ejected electron energies are listed in Table V.

TABLE III. Photoionization cross sections σ of the unscreened Be^+, B^{2+}, and C^{3+} ions obtained in our present work are compared to other results. ϵ is the energy of the ejected electron.

		σ (units of a_0^2)			
	ϵ (a.u.)	Present results	P_M[a]	P_R[b]	N[c]
Be^+	0.00	5.684(−2)	5.728(−2)	5.711(−2)	
	0.40	3.023(−2)	3.048(−2)	3.052(−2)	
	0.80	1.773(−2)	1.785(−2)	1.801(−2)	
	1.20	1.136(−2)	1.138(−2)	1.158(−2)	
B^{2+}	0.00	3.593(−2)	3.596(−2)	3.603(−2)	
	0.45	2.304(−2)	2.308(−2)	2.315(−2)	
	0.90	1.570(−2)	1.572(−2)	1.583(−2)	
	1.80	8.352(−3)	8.336(−3)	8.478(−3)	
C^{3+}	0.00	2.350(−2)	2.346(−2)	2.353(−2)	2.349(−2)
	0.48	1.715(−2)	1.713(−2)	1.720(−2)	1.709(−2)
	0.80	1.417(−2)	1.416(−2)	1.422(−2)	1.415(−2)
	1.60	9.281(−3)	9.266(−3)	9.340(−3)	9.324(−3)

[a]The model potential calculations by Peach *et al.* in Ref. [7].
[b]The *R*-matrix results by Peach *et al.* in Ref. [7].
[c]The work by Nahar and Pradhan in Ref. [27].

TABLE IV. Photoionization cross sections σ of the unscreened N^{4+}, O^{5+}, and F^{6+} ions obtained in our present work are compared to other results. ϵ is the energy of the ejected electron.

		σ (units of a_0^2)			
	ϵ (a.u.)	Present results	P_M[a]	P_R[b]	N[c]
N^{4+}	0.00	1.633(−2)	1.630(−2)	1.635(−2)	1.629(−2)
	0.15	1.520(−2)		1.523(−2)	1.517(−2)
	0.25	1.451(−2)	1.448(−2)	1.454(−2)	
	0.30	1.417(−2)		1.421(−2)	1.414(−2)
	0.75	1.162(−2)	1.161(−2)	1.166(−2)	1.162(−2)
	1.25	9.480(−3)	9.466(−3)	9.524(−3)	
O^{5+}	0.00	1.193(−2)	1.190(−2)	1.196(−2)	1.193(−2)
	0.36	1.053(−2)	1.051(−2)	1.056(−2)	
	0.40	1.039(−2)		1.042(−2)	1.039(−2)
	0.72	9.355(−3)	9.334(−3)	9.382(−3)	
	0.80	9.117(−3)		9.145(−3)	9.099(−3)
	1.08	8.350(−3)	8.333(−3)	8.379(−3)	
	1.20	8.048(−3)		8.078(−3)	8.056(−3)
F^{6+}	0.00	9.077(−3)		9.094(−3)	8.945(−3)
	0.37	8.227(−3)		8.245(−3)	8.127(−3)
	0.74	7.484(−3)		7.503(−3)	7.406(−3)
	1.11	6.831(−3)		6.851(−3)	6.767(−3)

[a]The model potential calculations by Peach *et al.* in Ref. [7].
[b]The *R*-matrix results by Peach *et al.* in Ref. [7].
[c]The work of N^{4+} by Nahar and Pradhan in Ref. [27]; the results of O^{5+} and F^{6+} by Nahar in Ref. [28] and Ref. [29], respectively.

It has been well known that with the exception of lithium, Cooper minima were discovered for ground-state photoionization of all the alkali-metal atoms [8]. The phenomenon of zeros in the dipole matrix element resulting in the appearance of Cooper minima in cross-section curves was interpreted

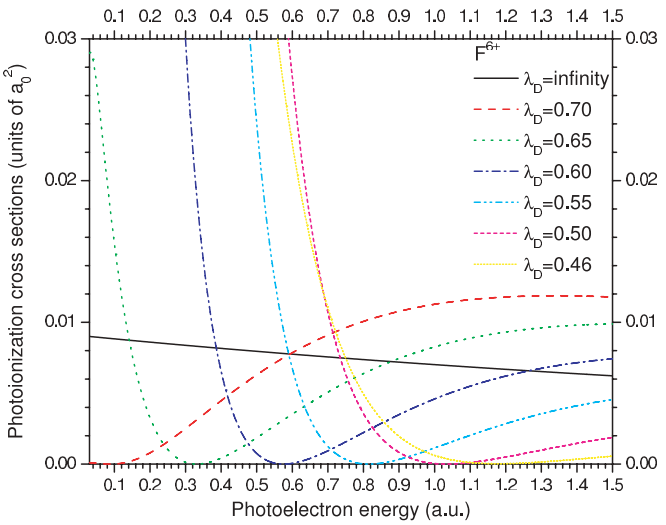

FIG. 13. (Color online) Photoionization cross sections of the ground state of F^{6+} ions varied with different Debye screening lengths λ_D (units of a_0).

TABLE V. Photoionization cross sections σ of lithium isoelectronic sequence for the selected Debye screening lengths λ_D. ϵ is the energy (in a.u.) of the ejected electron.

		σ (units of a_0^2)					
	λ_D (units of a_0)	$\epsilon = 1.0$	$\epsilon = 1.5$	$\epsilon = 2.0$	$\epsilon = 2.5$	$\epsilon = 3.0$	$\epsilon = 3.5$
Be^+	1.8	1.036(−2)	5.727(−3)	3.491(−3)	2.298(−3)	1.595(−3)	1.158(−3)
	2.2	1.416(−2)	7.829(−3)	4.815(−3)	3.222(−3)	2.280(−3)	1.690(−3)
	3.0	1.712(−2)	9.480(−3)	5.833(−3)	3.872(−3)	2.716(−3)	1.987(−3)
B^{2+}	1.2	1.153(−2)	7.691(−3)	5.201(−3)	3.663(−3)	2.680(−3)	2.024(−3)
	1.5	1.815(−2)	1.170(−2)	7.852(−3)	5.522(−3)	4.040(−3)	3.054(−3)
	1.8	2.133(−2)	1.360(−2)	9.142(−3)	6.449(−3)	4.734(−3)	3.588(−3)
C^{3+}	0.80	4.636(−3)	4.326(−3)	3.349(−3)	2.585(−3)	2.028(−3)	1.589(−3)
	1.0	1.362(−2)	1.076(−2)	8.024(−3)	6.039(−3)	4.641(−3)	3.641(−3)
	1.3	2.126(−2)	1.548(−2)	1.132(−2)	8.482(−3)	6.517(−3)	5.122(−3)
N^{4+}	0.65	2.217(−3)	3.512(−3)	3.255(−3)	2.753(−3)	2.266(−3)	1.875(−3)
	0.80	1.006(−2)	9.991(−3)	8.326(−3)	6.727(−3)	5.438(−3)	4.437(−3)
	1.0	1.823(−2)	1.511(−2)	1.198(−2)	9.510(−3)	7.633(−3)	6.210(−3)
O^{5+}	0.60	1.931(−3)	4.756(−3)	5.038(−3)	4.572(−3)	3.972(−3)	3.406(−3)
	0.75	1.121(−2)	1.160(−2)	1.025(−2)	8.701(−3)	7.323(−3)	6.176(−3)
	0.84	1.536(−2)	1.412(−2)	1.202(−2)	1.005(−2)	8.405(−3)	7.069(−3)
F^{6+}	0.55	1.134(−3)	4.558(−3)	5.510(−3)	5.386(−3)	4.922(−3)	4.386(−3)
	0.65	8.267(−3)	9.888(−3)	9.503(−3)	8.545(−3)	7.509(−3)	6.554(−3)
	0.70	1.127(−2)	1.178(−2)	1.083(−2)	9.565(−3)	8.329(−3)	7.234(−3)

by Bates [30,31], and then further explained by Seaton [32] and Cooper [33]. Later Manson [34] gave a systematic study showing that Cooper minima occur for all subshells whose wave functions have nodes, except the 2*s* subshell. The basic mechanism responsible for such phenomenon is the relative distribution of radial wave functions between discrete and continuum states, which leads to a sign change in the dipole matrix element with the variation of photon energies. The previous research on photoionization processes in Debye plasmas by Sahoo and Ho [10] reported that Cooper minima are uncovered for photoionization of plasma-embedded lithium due to plasma screening effects. Compared to the unscreened ions, a change in quantum defect and deviation from the Coulomb phase shift for the discrete and continuum state, respectively, are introduced through the screening of plasmas modifying the relative distribution of wave functions. As the screening effects are increased, the ground-state wave functions become diffuse and the ground-state energies are increased. In other words, the deviation of wave functions from unscreened ions, which raises the instability of ground state, increases the possibility for the dipole matrix elements to have zero values. In Fig. 14, the scaled ground-state energies and the locations of Cooper minima varied with the inverse Debye screening length for Li-like ions are given, in which the energies are scaled by a factor of $Z-2$ in order to better present all results in one figure. As mentioned, the ground-state energies are increased with decreasing of Debye screening lengths for each ion, but the higher Z cases need the stronger plasma screening to completely shift the ground states into continua. The Cooper minima are dependent significantly on the screening effects and only exist for a certain range of Debye screening lengths. With the increase of screening effects, the locations of Cooper minima move away from the thresholds toward the higher energies. This phenomenon can be understood as following. While the screening effects are enhanced causing continuum wave functions diffused more than discrete wave functions, for example, referring to Figs. 1 and 2 in Ref. [13], the higher photoelectron energies, on the contrary, lead to the

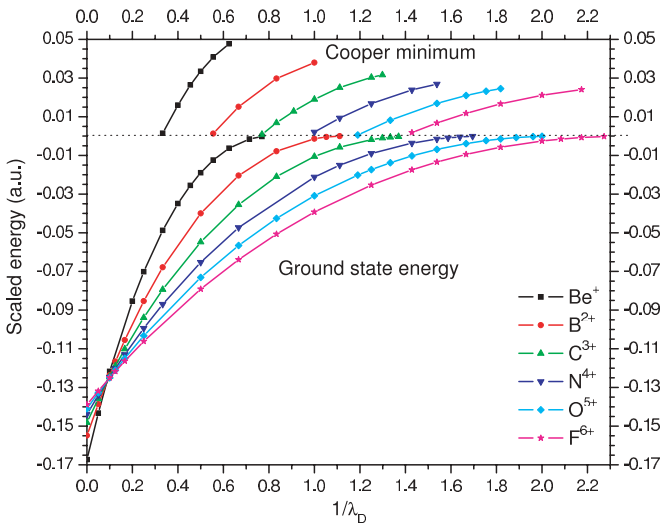

FIG. 14. (Color online) Locations of Cooper minima with respect to ionization thresholds (upper panel) and ground-state energies (lower panel) both scaled by a factor of $Z-2$ as functions of the inverse Debye screening lengths $1/\lambda_D$ (units of a_0^{-1}) for Li-like ions.

TABLE VI. Critical Debye screening lengths λ_D^c for Cooper minima starting to appear and critical values of Debye screening lengths λ_D^g for ground states shifting into continua.

	$\lambda_D{}^c$ (units of a_0)	$\lambda_D{}^g$ (units of a_0)
Be^+	3.0	1.3
B^{2+}	1.8	0.90
C^{3+}	1.3	0.70
N^{4+}	1.0	0.58
O^{5+}	0.84	0.49
F^{6+}	0.70	0.43

contraction of continuum wave functions. The phase shift of continuum wave function due to the stronger plasma screening effect is compensated by the phase shift due to the higher photon energy. Therefore, the negative and positive portions of the dipole matrix element could entirely be canceled at some higher photon energy for the more intense screening effect. The critical Debye screening lengths $\lambda_D{}^c$, at which the Cooper minimum starts to appear, and $\lambda_D{}^g$, the critical value of screening length to support the bound ground state, are listed in Table VI for each ions. The region of Debye screening lengths between $\lambda_D{}^c$ and $\lambda_D{}^g$ provides the limit of plasma conditions for the Cooper minima to exist in the ground states of Li-like ions.

IV. CONCLUSIONS

The method of complex coordinate rotation combined with the model potential approximation is adopted to investigate the screening effects of the Debye-Hückel–type potential on photoionization of plasma-embedded Li-like ions. The calculated photoionization cross sections without plasma screening disturbance are compared to the existing theoretical predictions for each considered ion and in excellent agreement with the most results. The photoionization cross sections varied with different Debye screening lengths illustrate the significant influence of plasma environments on photoionization for low photon energies, particularly the region near thresholds. The existence of a Cooper minimum depends mainly on relative distribution or phase difference of discrete and continuum wave functions. Its location shifts toward higher energy with decreasing Debye screening lengths. The instability of the ground states caused by the decrease of Debye screening lengths is related to the appearance of Cooper minima. Two critical screening lengths $\lambda_D{}^c$ and $\lambda_D{}^g$ for each considered ions in Table VI give the upper and lower limits of screening lengths, respectively, which confine the existence of Cooper minima.

ACKNOWLEDGMENTS

Financial support by the National Science Council of Taiwan (Republic of China) is gratefully acknowledged.

[1] D. W. Savin, in *Spectroscopic Challenges of Photoionized Plasmas*, Vol. 247, edited by G. J. Ferland and D. W. Savin (Astronomical Society of the Pacific, San Francisco, 2001), p. 167.
[2] K. L. Bell, Phys. Scr. **T100**, 64 (2002).
[3] R. Indebetouw and J. M. Shull, Astrophys. J. **605**, 205 (2004).
[4] G. McGinn, J. Chem. Phys. **53**, 3635 (1970).
[5] J. A. Tully, Astrophys. J. **288**, 831 (1985).
[6] R. E. H. Clark, R. D. Cowan, and F. W. Bobrowicz, At. Data Nucl. Data Tables **34**, 415 (1986).
[7] G. Peach, H. E. Saraph, and M. J. Seaton, J. Phys. B: At. Mol. Opt. Phys. **21**, 3669 (1988).
[8] G. V. Marr and D. M. Creek, Proc. R. Soc. London. Ser. A **304**, 233 (1968).
[9] L. B. Zhao and Y. K. Ho, Phys. Plasmas **11**, 1695 (2004).
[10] S. Sahoo and Y. K. Ho, Phys. Plasmas **13**, 063301 (2006).
[11] S. Sahoo and Y. K. Ho, J. Quant. Spectrosc. Radiat. Transfer **111**, 52 (2010).
[12] S. Sahoo and Y. K. Ho, Res. Lett. Phys. **2009**, 832413 (2009).
[13] Y. Y. Qi, Y. Wu, and J. G. Wang, Phys. Plasmas **16**, 033507 (2009).
[14] J. T. Broad and W. P. Reinhardt, J. Chem. Phys. **60**, 2182 (1974).
[15] T. N. Rescigno and V. McKoy, Phys. Rev. A **12**, 522 (1975).
[16] W. P. Reinhardt, Annu. Rev. Phys. Chem. **33**, 223 (1982).
[17] B. R. Johnson and W. P. Reinhardt, Phys. Rev. A **28**, 1930 (1983).
[18] Y. K. Ho, Phys. Rep. **99**, 1 (1983).
[19] A. Buchleitner, B. Gremaud, and D. Delande, J. Phys. B: At. Mol. Opt. Phys. **27**, 2663 (1994).
[20] C. V. Sukumar and K. C. Kulander, J. Phys. B: At. Mol. Phys. **11**, 4155 (1978).
[21] T. K. Fang and Y. K. Ho, Phys. Rev. A **60**, 2145 (1999).
[22] H. Bachau, P. Galan, and F. Martin, Phys. Rev. A **41**, 3534 (1990).
[23] S. Bashkin and J. O. Stoner, *Atomic Energy Levels and Grotrian Diagrams*, Vol. 1 (North-Holland, Amsterdam, 1975).
[24] C. A. Rouse, Phys. Rev. A **4**, 90 (1971).
[25] J. C. Stewart and K. D. Pyatt, Astrophys. J. **144**, 1203 (1966).
[26] B. J. B. Crowley, Phys. Rev. A **41**, 2179 (1990).
[27] S. N. Nahar and A. K. Pradhan, Astrophys. J. Suppl. Ser. **111**, 339 (1997).
[28] S. N. Nahar, Phys. Rev. A **58**, 3766 (1998).
[29] S. N. Nahar, Astrophys. J. Suppl. Ser. **164**, 280 (2006).
[30] D. R. Bates, Mon. Not. R. Astron. Soc. **106**, 432 (1946).
[31] D. R. Bates, Proc. R. Soc. London. Ser. A **188**, 350 (1947).
[32] M. J. Seaton, Proc. R. Soc. London. Ser. A **208**, 418 (1951).
[33] J. W. Cooper, Phys. Rev. **128**, 681 (1962).
[34] S. T. Manson, Phys. Rev. A **31**, 3698 (1985).